Pathways for SO_2 dissociation on Cu(100): density functional theory

2007 J. Phys.: Condens. Matter 19 365244

(http://iopscience.iop.org/0953-8984/19/36/365244)

IOP PUBLISHING JOURNAL OF PHYSICS: CONDENSED MATTER

J. Phys.: Condens. Matter **19** (2007) 365244 (12pp) doi:10.1088/0953-8984/19/36/365244

Pathways for SO_2 dissociation on Cu(100): density functional theory

Romel Mozo[1,2], Mohammad Kemal Agusta[1], Md Mahmudur Rahman[1,5], Wilson A Diño[2,3,4], Emmanuel T Rodulfo[2] and Hideaki Kasai[1]

[1] Department of Precision Science and Technology and Applied Physics, Osaka University, 2-1 Yamadaoka, Suita, Osaka 565-0871, Japan
[2] Physics Department, De La Salle University, Taft Avenue, Manila 1004, Philippines
[3] Department of Physics, Osaka University, Toyonaka, Osaka 560-0043, Japan
[4] Center for the Promotion of Research on Nanoscience and Nanotechnology, Osaka University, Toyonaka, Osaka 560-8531, Japan

E-mail: rahman@dyn.ap.eng.osaka-u.ac.jp

Received 11 July 2007, in final form 12 July 2007
Published 24 August 2007
Online at stacks.iop.org/JPhysCM/19/365244

Abstract

The dissociation of SO_2 on Cu(100) and the diffusion of the co-adsorbed decomposition products S and O were investigated using density functional theory-based calculations. Two dissociation pathways were considered: (P1) $SO_2 \rightarrow O + SO \rightarrow S + 2O$ and (P2) $SO_2 \rightarrow S + 2O$, the difference being in the formation of the intermediate product SO. It is found that P1 is favored kinetically with a total effective dissociation barrier of 0.78 eV compared to P2 which has 1.58 eV. The transition state leading to the formation of O + SO is found to be a result of the weakened interaction between the O of SO and the surface while the transition state for breaking SO is seen to be that of the repulsive nature of co-adsorbed S and O. The co-adsorbed S has a lower diffusion barrier of 0.41 eV compared to O which has a barrier ranging from 0.49 to 0.95 eV.

1. Introduction

The interaction of SO_2 with metals and metal oxides has been investigated primarily because of the industrial importance of SO_2 (for sulfuric acid production) and the harmful effects it brings when released to the environment. It has also attracted interest in other fields including catalyst poisoning, automobile emission control, and metal corrosion [1, 2].

On the other hand, copper is used in many applications ranging from electronic devices to roofs and statues [3]. Usually supported on metal oxides, it is used as a catalyst in

[5] Author to whom any correspondence should be addressed.

industrial processes where it interacts directly with SO_2, e.g. the Claus reaction and reduction of SO_2 by CO ($SO_2 + 2CO \rightarrow 2CO_2 + S_n$) [4]. Surprisingly, although there have been several experimental investigations on SO_2–Cu interactions [5–10], rarely can we find theoretical studies in the literature.

Previous experimental studies have focused primarily on the determination of the geometry of adsorbed SO_2, and the identification and geometry of its decomposition products [5–10]. At low temperature (170 K), SO_2 adsorbs molecularly on Cu surfaces [5, 7]. Increasing the temperature to about room temperature or, alternatively, allowing this molecule to be adsorbed at this temperature, yields decomposition products identified as O, S, SO and SO_3 [5–10]. Increasing the temperature further results in recombination and desorption from the surface. To account the different observations, several reaction mechanisms were proposed:

$$SO_2(a) \rightarrow SO(a) + O(a) \quad (1)$$

$$SO(a) \rightarrow S(a) + O(a) \quad (2)$$

$$SO_2(a) + O(a) \rightarrow SO_3(a) \quad (3)$$

$$SO_2(a) + SO(a) \rightarrow SO_3(a) + S(a) \quad (4)$$

$$SO_2(a) \rightarrow S(a) + 2O(a) \quad (5)$$

$$3SO_2(a) \rightarrow 2SO_3(a) + S(a). \quad (6)$$

Recently, theoretical calculations were performed to determine the energetics and geometry of SO_2 adsorbed on Cu surfaces [4, 11]. For small coverages, the stability on Cu(100) increases in the order η^1-S $<$ η^2-S, O $<$ η^2-O, O $<$ η^3-S, O, O bonding modes [4]. Thermochemical calculation reveals that it is easier to generate SO_3 ($3SO_2 \rightarrow 2SO_3 + S$) than SO ($SO_2 \rightarrow SO + O$) as an intermediate to SO_2 decomposition [4]. On Cu(111), an SO_2 lying perpendicular to the surface with the O atoms located on the top sites is found to be the most stable structure [11]. But the question as to how dissociation proceeds remains untackled and unanswered.

In this study, we investigated the adsorption and dissociation of SO_2 on Cu(100) within the framework of density functional theory (DFT). On the basis of the different proposed reactions, we considered two dissociation pathways for which the final products are co-adsorbed S and O atoms. These pathways are denoted as (P1) $SO_2 \rightarrow O + SO \rightarrow S + 2O$, which represents a succession of reactions (1) and (2), and (P2) $SO_2 \rightarrow S + 2O$, which is just reaction (5). The difference of the two pathways lies in the formation of SO as an intermediate product. Pathway P1 (or the reactions therein) has been proposed based on XPS and EELS [5, 7] while P2, although considered to be a minor process occurring, may likely describe reaction (6), known in the literature as the disproportionation reaction (think that each of the two dissociated O combines with the neighboring SO_2 to produce SO_3). This disproportionation reaction has been observed to occur quantitatively upon room temperature adsorption based on AES and XPS results [6, 10].

2. Computational details

All electronic properties were evaluated within the DFT formulation. The Kohn–Sham one-electron valence states were expanded in a plane wave basis set of energy below 26 Ryd while the ionic core was described by ultrasoft pseudopotentials [12]. The generalized gradient approximation of Perdew and Wang (GGA-PW91) [13] was used for the exchange–correlation energy. The Cu(100) slab was modeled by three atomic layers and a vacuum space equivalent to seven atomic layers was used to minimize the interaction between the image slabs. Previous studies have shown that a three-layer Cu slab is enough to describe the properties of the bare

Table 1. Structural parameters for adsorbed or co-adsorbed SO_2, SO, S and O, and binding stabilities E_b, calculated relative to the sum of the energies of isolated substrate and isolated SO_2 molecule ($E_b = E_{sys} - E_{Cu} - E_{SO_2}$).

Structure	S–O bond length (Å)	O–S–O bond angle (deg)	E_b (eV)
	(A) SO_2		
(1) η^1-S hollow	1.49	117	+0.06
(2) η^2-O, O two bridges (2B)	1.59	106	−0.60
(3) η^2-O, O long bridge (LB)	1.54	112	−0.36
(4) η^2-O, O short bridge (SB)	1.54	111	−0.51
	(B) SO + O		
(1)	1.67	—	−0.38
(2)	1.68	—	−0.71
	(C) S + 2O		
(1)	—	—	−0.27
(2)	—	—	−0.01
(3)	—	—	−1.15
(4)	—	—	−1.23

slab and the energetics of atomic or molecular adsorption [4, 14–16]. The adsorption and dissociation of SO_2 were investigated by placing the molecule in a p(3 × 2) unit cell. This corresponds to a coverage of $\theta_{SO_2} = 1/6$, which is very close to that observed using NEXAFS experiment (0.15 ± 0.01) [6]. The surface Brillouin zone was sampled using a 6 × 4 mesh of the Monkhorst and Pack scheme [17]. Convergence with respect to the choice of k-points was checked against a denser mesh. Calculation for the gas phase SO_2 gives a S–O bond length of 1.47 Å and a bond angle of 119°, in very good agreement with the experimental values of 1.43 Å and 119° [18]. Owing to computational cost, all substrate atoms were fixed at the bulk geometry corresponding to the experimental lattice constant of 3.61 Å [19].

3. Results

3.1. Adsorbate geometries

In choosing appropriate initial or final geometry of the adsorbates, different initial adsorption geometries were considered.

3.1.1. SO_2. Although, in general, SO_2 can bind either through one, two or all of its atoms, we focused on the bonding mechanisms for which the two O atoms of the molecule are equivalent or located on similar sites. These bonding mechanisms, although primarily chosen to systematically study the dissociation processes, have shown high adsorption stability [4] (except for configuration (1) η^1-S). The investigated adsorption geometries are: (1) η^1-S, (2) η^2-O, O *on two bridges*, (3) η^2-O, O *on a long bridge*, and (4) η^2-O, O *on a short bridge* (figure 1(A)). The present calculation shows that the molecule lies perpendicular to the surface, in agreement with the previous studies [4, 8, 10]. The structural parameters and the stability E_b, defined as the difference between the energy of the adsorbate–substrate system and the sum of the energies of isolated substrate and isolated SO_2 molecule ($E_b = E_{sys} - E_{Cu} - E_{SO_2}$), are listed in table 1.

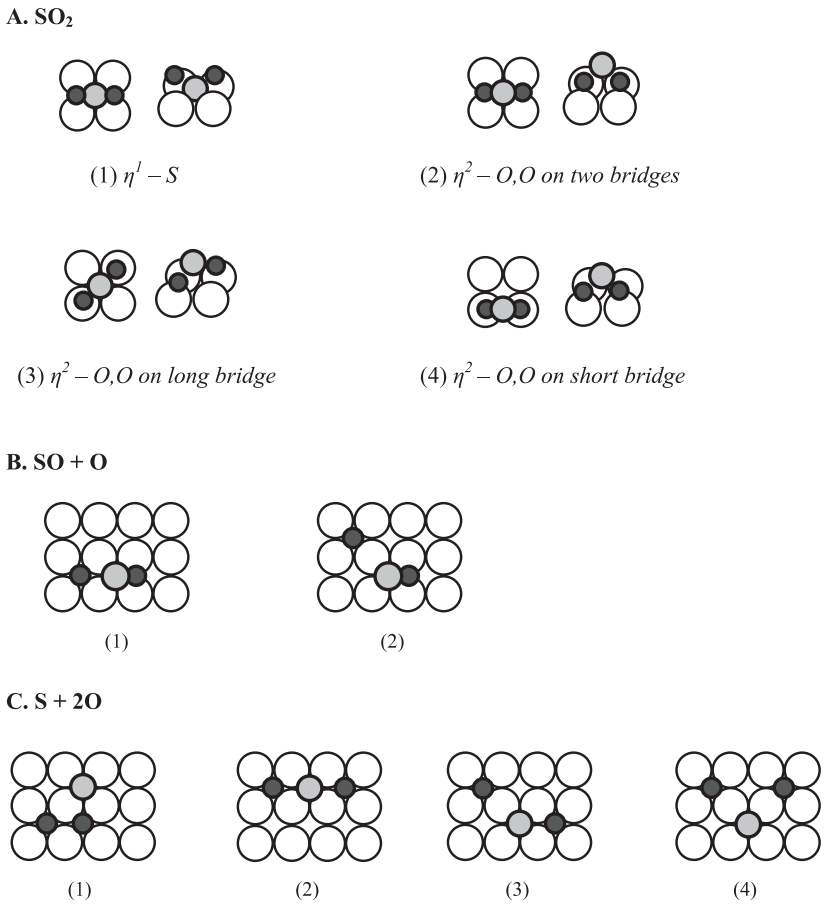

Figure 1. Different stable configurations for adsorbed or co-adsorbed SO_2, SO, S and O. For clarity, the periodic images are not shown. In the optimized structures, the O and S atoms are slightly off exact hollow or bridge sites.

3.1.2. SO + O. Figure 1(B) shows two of the many possible stable structures for the co-adsorption of SO and O. Other initial configurations (not shown), e.g. O at atop or bridge sites, were tested and found the structures unstable which spontaneously transform towards the shown configurations after full relaxation. In all cases, the O prefers hollow sites in consistency with a previous study on O chemisorption [20]. The SO molecule lies almost perfectly flat on the surface with an average tilt of ∼4° for which the S lies near hollow sites and the O slightly crosses the bridge sites. Pangher and co-workers [8] were able to observe, using an XAFS experiment, a flat-lying SO molecule which bonds to the surface through both S and O atoms. The S atoms are located in hollow sites while the O atoms are nearly bridging two Cu atoms. However, the co-adsorbed O was observed to lie on the bridge site.

3.1.3. S + 2O. Four geometries for the co-adsorption of S and 2O were explored in the calculations (figure 1(C)). Other initial geometries were likewise tested and hollow site preference of the adatoms found. The result is consistent with previous studies on S adsorption or co-adsorption [6, 21–23]. It can be noted from the values of the stability in table 1 that as the distance between co-adsorbed S and O increases, the value of the stability increases. An

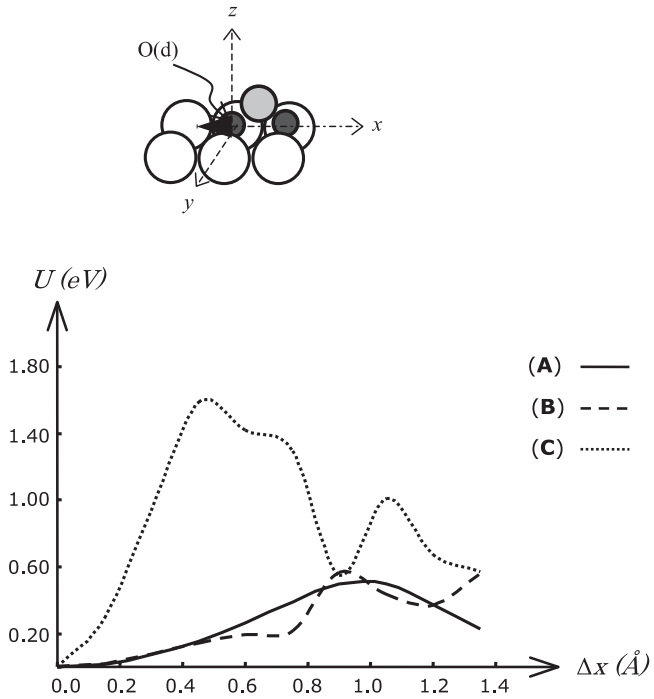

Figure 2. Model for the dissociation process $SO_2 \rightarrow SO + O$ (top) and energy profiles for processes (A) $SO_2(a) \rightarrow O(a) + SO(a)$, (B) $O(a) + SO(a) \rightarrow S(a) + 2O(a)$ and (C) $SO_2(a) \rightarrow S(a) + 2O(a)$ (bottom). The reference energy for (A) and (C) is the energy for configuration A-2 (figure 1) while for (B) it is that of configuration B-1.

assumption therefore can be made that a repulsive interaction exists between these two adatoms, a situation commonly observed for adsorbate–adsorbate interaction.

3.2. Dissociation results

To determine which pathway is favored, the dissociation barrier in each dissociation step (two steps in P1 and only one step for P2) is obtained. Hereafter, we use the following symbols: O for the oxygen attached to S, O(a) for the co-adsorbed oxygen, O(d) for the dissociating oxygen, and S(a) for the co-adsorbed S.

3.2.1. Pathway P1.

(1) $SO_2(a) \rightarrow SO(a) + O(a)$

As suggested from the results in section 1.A, we chose the starting geometry of $SO_2(a)$ as shown in figure 1(A)-2. For the dissociation process, one of the oxygen atoms, O(d) in this case, is constrained to move away from SO, an increment of 0.15 Å along x (figure 2, top) while allowing it to relax along the remaining orthogonal degrees of freedom (y and z directions). The remaining S and O were fully relaxed. With this model, the dissociating molecule can freely rotate and translate subject to a constraint—O(d) is free to translate within the yz plane only. Moreover, the final co-adsorbed state may either end up with configuration B-1 or B-2 (figure 1), assuming dissociation occurs as predicted. Also, this model may actually represent $SO_2(a)$ diffusion if, in the course of moving O(d), the

molecule remains intact. The energy variation with respect to O(d) x displacement is shown in figure 2, curve A. The process ends up to dissociation with SO(a) and O(a) as products described in configuration B-1. The barrier to dissociation is 0.50 eV. Before the transition state (TS1) is reached, it is observed that as O(d) moves, the SO continually follows, keeping the S–O(d) and S–O bond lengths almost the same as the initial (1.59 Å). At TS1, the bond lengths are a little bit shorter (S–O(d) = 1.56 Å, S–O = 1.50 Å). However, the height of O above the surface is drastically increased to $z = 3.0$ Å (from an initial of 1.71 Å), the same height as S (S–O is parallel to the surface at TS1). This observation may indicate that the origin of the barrier may arise from the weakening of the O–Cu bonding. Throughout the entire process, the O(d)–SO system did not exhibit any rotation within the plane of the surface implying that rotation is an activated process.

(2) $O(a) + SO(a) \rightarrow S(a) + 2O(a)$

A model similar to that described above is used for the dissociation process $O(a) + SO(a) \rightarrow S(a) + 2O(a)$, i.e. the O(d) is constrained to move away from S. We note again that the final position of O(d) is not predetermined since the S–O(d) system may be free to rotate and translate. In a like manner, the model may well represent SO diffusion, if SO remains intact throughout the process. From the data, we observed that as O(d) moves, the S atom adjusts, keeping the S–O(d) bond length almost constant (∼1.7 Å) until the transition state (TS2) is reached. At TS2, unlike for reaction (1), it is the S–O(d) bond length that is significantly stretched to 2.50 Å while the height of these atoms changes only slightly. The S–O(d) system also did not exhibit any rotation within the plane of the surface implying an activated rotation. The final co-adsorbed products have the configuration shown in figure 1(C)-2. The energy variation with respect to the O(d) displacement is shown in figure 2, curve B. The dissociation barrier for this process is 0.56 eV.

3.2.2. Pathway P2. $SO_2(a) \rightarrow S(a) + 2O(a)$.

Here, two O(d) are simultaneously constrained to move away from S. As expected from the symmetric motion of the two O(d), the S atom remains in the same lateral position, with only the height changing, throughout the course of the dissociation process. The resulting energy variation with respect to the displacement of O(d) is displayed in figure 2(C). The barrier for this process is 1.58 eV. As can be seen, the curve shows a feature of a stable undissociated SO_2 after the transition state is crossed.

3.2.3. Unrelaxed adsorbate model. Out of curiosity, we also tried to estimate the dissociation barrier for reaction (1) of P1 and for P2 by varying the S–O bond length $\boldsymbol{r}$ at different bond angles $\boldsymbol{\theta}$ (figure 3, top). For reaction (1), one oxygen atom (O(d)) is constrained to be stretched (or compressed) by an increment of 0.2 Å from the equilibrium bond length at a given value of $\boldsymbol{\theta}$ ($\boldsymbol{r}$ for this case ranges from 1.39 to 3.99 Å). The $\boldsymbol{\theta}$ in turn is varied from 51° to 58° at an increment of 0.5°. The result will give us an idea as to the sensitivity of the energy with respect to bond stretching and bond bending, which are important parameters for any dissociation process. The resulting potential energy surface (PES; figure 3, bottom left) shows strong sensitivity of the energy to $\boldsymbol{r}$ within the range of $\boldsymbol{\theta}$ considered. The estimated value of the dissociation barrier is 1.56 eV (bottom right figure). This value is close to that estimated in [4] (∼1.73 eV) which uses a starting geometry of SO_2 on the hollow (η^2-S, O) and ends at O on the bridge and SO on the hollow (η^2-S, O). For reaction (2), both of the S–O bond lengths are simultaneously changed while keeping S at its initial position. A similar PES is obtained (not shown) but with a very high dissociation barrier of 3.17 eV. The resulting trend

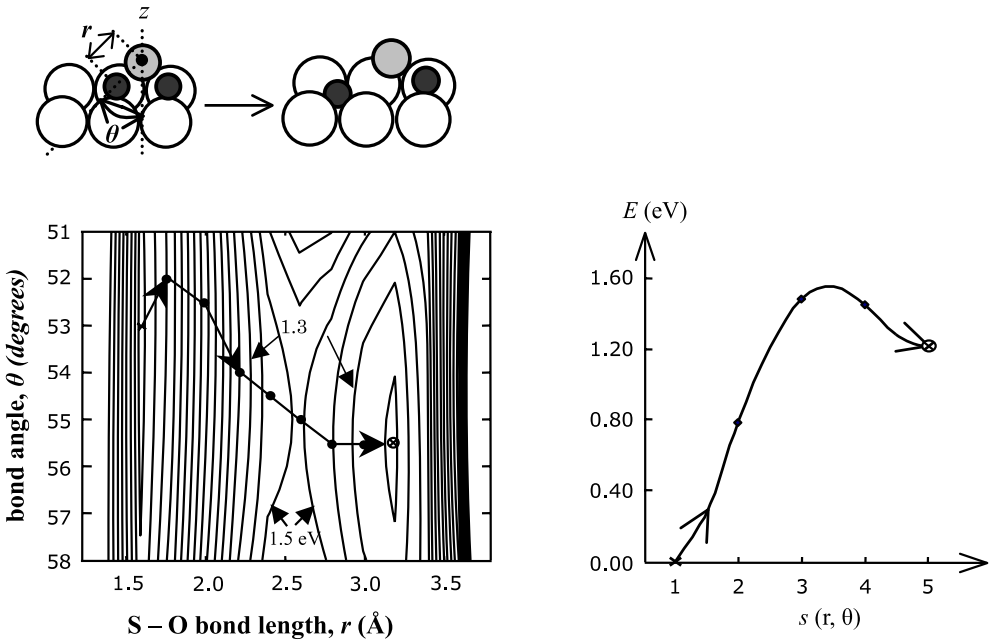

Figure 3. Model for $SO_2 \rightarrow SO + O$ dissociation having fixed adsorbate position (top figure); potential energy surface having a contour spacing of 0.1 eV (bottom left). The arrow shown traces the minimum energy path s for the dissociation process. The energy variation along this path is displayed in the right figure. The selected five points in s have coordinates $(r, \theta) = (1.59, 53.0)$, (1.99, 52.5), (2.39, 54.5), (2.79, 55.5) and (3.19 Å, 55.5°). The reference energy corresponds to the energy of the most stable SO_2 on Cu(100). The points marked $\times$ and $\otimes$ represent initial and final configurations, respectively.

in the values of the dissociation barrier is in agreement with the model described in sections A-1 and B.

3.3. Atomic adsorbate diffusion

The result in section 2.A-1 shows that the dissociation of SO_2 ends up with SO(a) + O(a) having the configuration shown in B-1 (figure 1) though it has less stability than B-2. In attaining configuration B-2, we investigate the diffusion of O(a) starting from configuration B-1. The barrier for this diffusion process is 0.82 eV. Similarly, the result in section 2.A-2 shows SO(a) ending up at S(a) + O(a) having the configuration shown in C-2, which is very less stable. Reaching the most stable configuration C-4 can be attained in two ways: either by allowing S or allowing the two O(a) to diffuse. Diffusion of S is activated by 0.41 eV while diffusion of the first and second O(a) gives 0.49 and 0.95 eV, respectively.

4. Discussion

The results above clearly indicate that the complete dissociation of SO_2 has to proceed via SO formation (pathway P1) with a total effective barrier of only 0.78 eV (figure 4) as compared to the direct complete dissociation (pathway (P2)) which has 1.58 eV. Aside from this very high barrier for P2, it is also observed that the system will encounter a stable undissociated state (deep relative minimum of curve C; figure 2) after crossing the barrier, thus making it

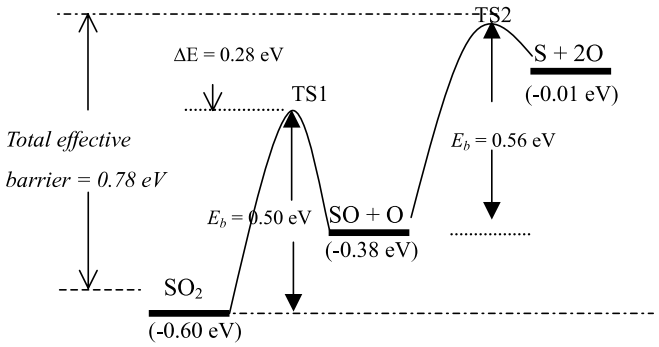

Figure 4. Energy diagram for the complete dissociation of SO_2. Energy values enclosed in parentheses represent the stability of the adsorbate–substrate system. Please see figure 1 and table 1 for details.

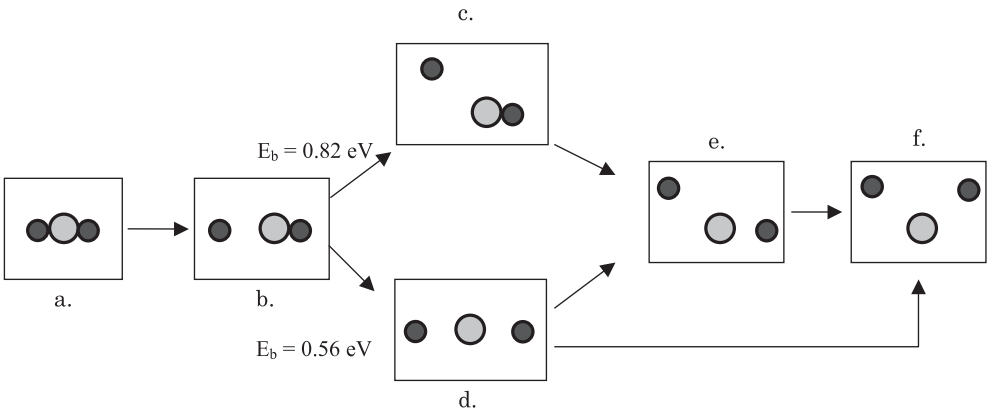

Figure 5. Possible routes for the complete dissociation of SO_2 to S + 2O. Configurations a to e are as described in the text.

difficult for this process to occur spontaneously. Qualitatively, our results are in good agreement with the experimental findings of Polcik and co-workers [7]. At low temperature (170 K), the dominant adsorbed species is molecular SO_2. Upon heating the SO_2-covered surface to about room temperature, SO_2 decomposes to SO(a) + O(a) + S(a). This behavior was also observed for SO_2 adsorbed on polycrystalline Zn using a photoemission study and on Zn(0001) using molecular orbital studies [24]. In contrast, Nakahashi and co-workers [6] observed that when SO_2 is adsorbed at room temperature, only SO_3 and S are detected from the surface at a ratio of $2SO_3$:1S, in quantitative agreement with the proposed disproportionation reaction. A careful look at figure 4 shows that the energy separating the two transition states (TS1 and TS2) is only $\Delta E = 0.28$ eV. Therefore, it is highly probable that beyond a certain temperature, probably just below room temperature, complete dissociation will proceed without completely passing the intermediate state SO(a) + O(a). On the basis of the present dissociation and diffusion results, we propose that any formation of SO_3 must be a result of either or both of the interactions between dissociated O, O(a), and the incoming SO_2(g), and between diffusing O(a) and SO_2(a) (SO_2 (gas or ads) + O(a) $\rightarrow$ SO_3(a)); this reaction has been previously suggested to occur [4]. Nakahashi *et al* [6] further observed that two distinct patterns are formed: a p(2 × 2) structure containing SO_3 species only, and a c(4 × 6) containing both S and SO_3, for

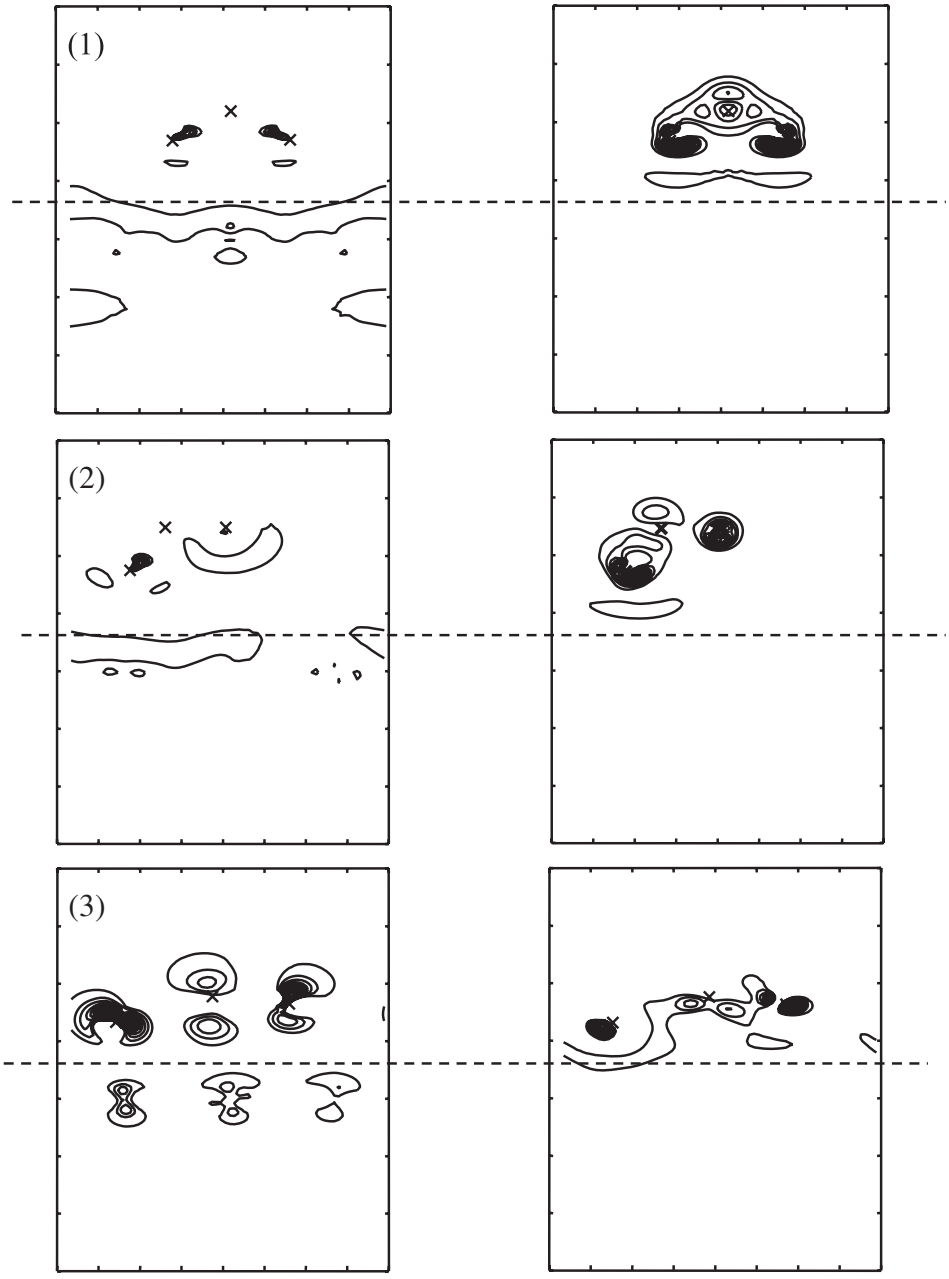

Figure 6. Charge density difference for the initial state of SO_2 (1), at TS1 (2), for O + SO (3), at TS2 (4), and for S + 2O (5). The plane is cut along the plane of OSO, i.e. the xz plane (see figure 2, top). The left panel shows the region of increased charge (+) while the right panel shows the region of decreased charge (−). Positions of the O and S atoms are marked with crosses. The dashed horizontal line represents the plane of the substrate atoms in the first layer. The contour spacing is 0.025 e A^{-3}.

which they conclude that the reactions products (including possibly SO) should migrate on the surface. The present result showed that it is unlikely for SO (and SO_2) to wholly diffuse on

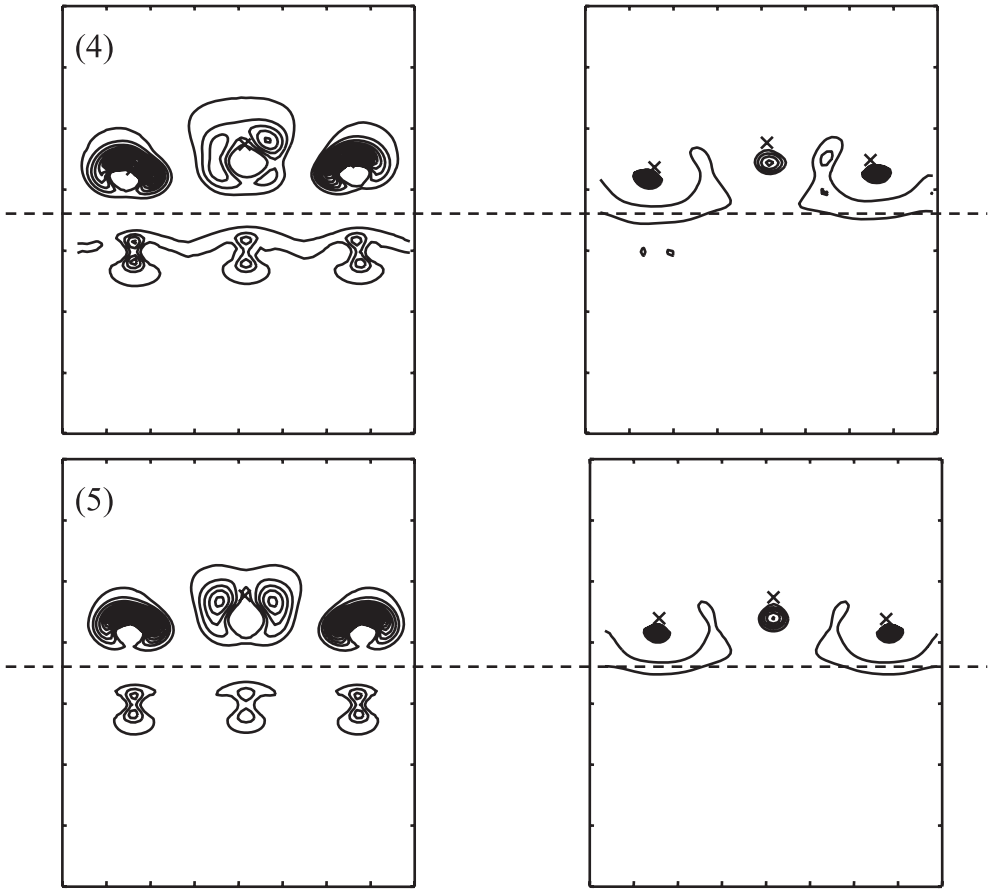

Figure 6. (Continued.)

the surface without being dissociated. Any difference in the observed patterns is most likely a result of the diffusion of atomistic adsorbates, particularly S which has a small diffusion barrier. Further, the present result also showed that complete dissociation has to take place first before any atomistic diffusion occurs. This is particularly depicted between path b to c, which represents an atomistic diffusion, and path b to d, which represents dissociation for which the former has a higher barrier compared to the latter (figure 5).

We will now turn our attention on how the electronic structure changes during the course of the entire dissociation process (from A-2 configuration to C-4 configuration of figure 1). Figure 6 shows a series of charge density differences, which are defined as the differences between the charge density of the adsorption system and the sum of the charge densities of the isolated substrate and isolated OSO distribution ($\Delta\rho = \rho_{\text{system}} - \rho_{\text{Cu}} - \rho_{\text{OSO}}$). The plot is along the plane of OSO (xz plane). For clarity, we divide the distribution into two regions: the region of increased (+) (left panel) and decreased (−) charge (right panel). The observed stability and the difference in the bond lengths and bond angle between adsorbed SO_2 and gaseous SO_2 can be explained by the charge transfer from the surface to the molecule with most of the charges being localized within the O atoms (figure 5(1)). This result is consistent with the fact that O has the largest electronegativity among the different atoms present. At

TS1, we recall that the bond lengths are O(d)–S = 1.56 Å and O–S = 1.50 Å. The latter bond length is almost the same as the calculated O–S bond length for gaseous SO_2 (1.47 Å). This result can be explained by looking at figure 5(2) for which we see that the O–S bonding is not modified by the surface interaction. From this observation, we conclude that the origin of the barrier must come from this O–surface weakened interaction, as suggested also by the height of O above the surface. We will now analyze the transition state for SO dissociation. We recall again in section 1.C that a repulsive nature of O(a) and S(a) interaction is deduced from the distance of the adsorbates and the corresponding value of the adsorption energy. A mere visual inspection of figure 5(4) (TS2) and figure 5(5) (final state of S(a) + 2O(a)) shows almost the same feature of charge redistribution. We conclude that the origin of the barrier must come from this repulsive behavior of the atoms. This behavior can be said to be a result of the competing reaction between S and O(d) on the Cu atoms for which both are bonded. Both atoms, being electronegative, take up electrons from the Cu atoms resulting in this repulsive behavior. A similar behavior was observed for CO oxidation on Pt(111) [25].

5. Conclusions

We have investigated the complete dissociation of SO_2 and the diffusion of the co-adsorbed products S and O within the framework of density functional theory. The barrier for the reaction $SO_2 \rightarrow O + SO$ is 0.50 eV, while for $O + SO \rightarrow S + 2O$ it is 0.56 eV. The overall effective barrier for this entire dissociation process is 0.78 eV. The origin of the first barrier is the weakened interaction between the O of SO and the surface, while the second barrier is due to the repulsive nature between co-adsorbed O and S. S diffuses more easily (barrier of 0.41 eV) than O (barrier between 0.49–0.95 eV).

Acknowledgments

This work was partly supported by a Grant-in-Aid for Scientific Research on Priority Areas (Developing Next Generation Quantum Simulators and Quantum-Based Design Techniques) from the Ministry of Education, Culture, Sports, Science and Technology, Japan. RM gratefully acknowledges the Japan Student Services Organization (JASSO) for financial assistance and the Department of Science and Technology—Philippine Council for Advanced Science and Technology Research and Development (DOST-PCASTRD), Philippines.

References

[1] Haase J 1997 *J. Phys.: Condens. Matter* **9** 3647
[2] Lu H, Janin E, Davila M E, Pradier C M and Göthelid M 1998 *Vacuum* **49** 171
[3] Samie F, Tidblad J, Kucera V and Leygraf C 2005 *Atmos. Environ.* **39** 7362
[4] Rodriguez J A, Ricart J M, Clotet A and Illas F 2001 *J. Chem. Phys.* **115** 454 and reference therein
[5] Leung K T, Zhang X S and Shirley D A 1989 *J. Phys. Chem.* **93** 6164
[6] Nakahashi T, Terada S, Yokoyama T, Hamamatsu H, Kitajima Y, Sakano M, Matsui F and Ohta T 1997 *Surf. Sci.* **373** 1
[7] Polcik M, Wilde L and Haase J 1996 *Phys. Rev.* B **53** 13720
[8] Pangher N, Wilde L, Polcik M and Haase J 1997 *Surf. Sci.* **372** 211
[9] Polcik M, Wilde L and Haase J 1998 *Phys. Rev.* B **57** 1868
[10] Jackson G J, Driver S M, Woodruff D P, Abrams N, Jones R G, Butterfield M T, Crapper M D, Cowie B C C and Formoso V 2000 *Surf. Sci.* **459** 231
[11] Sakai Y, Koyanagi M, Mogi K and Miyoshi E 2002 *Surf. Sci.* **513** 272
[12] Vanderbilt D H 1990 *Phys. Rev.* B **41** 7892

[13] Perdew J P, Chevary J A, Vosko S H, Jackson K A, Pederson M R, Singh D J and Fiolhais C 1992 *Phys. Rev.* B **46** 6671
[14] Gay J G, Smith J R and Arlinghaus F J 1977 *Phys. Rev. Lett.* **38** 561
[15] Nobuhara K, Kasai H, Nakanishi H and Diño W A 2004 *J. Appl. Phys.* **96** 5020
[16] Chena W, Lub C, Chena Z, Lia Y and Li J 2006 *Chin. J. Chem. Phys.* **19** 54
[17] Monkhorst H J and Pack J D 1976 *Phys. Rev.* B **13** 5188
[18] Chaturvedi S, Rodriguez J A, Jirsak T and Hrbek J 1998 *J. Phys. Chem.* B **102** 7033
[19] Ashcroft N W and Mermin D 1976 *Solid State Physics* Thomson Publishing
[20] Puisto A, Pitkänen H, Alatalo M, Jaatinen S, Salo P, Foster A S, Kangas T and Laasonen K 2005 *Catal. Today* **100** 403
[21] McGrath R, Macdowell A A, Hashizume T, Sette F and Citrin P H 1990 *Phys. Rev. Lett.* **64** 575
[22] Bahr C C, Barton J J, Hussain Z, Robey S W, Tobin J G and Shirley D A 1987 *Phys. Rev.* B **35** 3773
[23] Zeng H C, MacFarlane R A and Mitchell K A R 1989 *Phys. Rev.* B **39** 8000
[24] Chaturvedi S, Rodriguez J A, Jirsak T and Hrbek J 1998 *J. Phys. Chem.* **102** 7033
[25] Alavi A, Hu P, Deutsch T, Silvestrelli P L and Hutter J 1998 *Phys. Rev. Lett.* **80** 3650